Protein–Protein Interactions

Deutsche Ausgabe: DOI: 10.1002/ange.201511601
Internationale Ausgabe: DOI: 10.1002/anie.201511601

Probing the Small-Molecule Inhibition of an Anticancer Therapeutic Protein-Protein Interaction Using a Solid-State Nanopore

Dong-Kyu Kwak[+], Hongsik Chae[+], Mi-Kyung Lee[+], Ji-Hyang Ha, Gaurav Goyal, Min Jun Kim, Ki-Bum Kim, and Seung-Wook Chi**

Abstract: *Nanopore sensing is an emerging technology for the single-molecule-based detection of various biomolecules. In this study, we probed the anticancer therapeutic p53 transactivation domain (p53TAD)/MDM2 interaction and its inhibition with a small-molecule MDM2 antagonist, Nutlin-3, using low-noise solid-state nanopores. Although the translocation of positively charged MDM2 through a nanopore was detected at the applied negative voltage, this MDM2 translocation was almost completely blocked upon formation of the MDM2/GST-p53TAD complex owing to charge conversion. In combination with NMR data, the nanopore measurements showed that the addition of Nutlin-3 rescued MDM2 translocation, indicating that Nutlin-3 disrupted the MDM2/GST-p53TAD complex, thereby releasing MDM2. Taken together, our results reveal that solid-state nanopores can be a valuable platform for the ultrasensitive, picomole-scale screening of small-molecule drugs against protein–protein interaction (PPI) targets.*

Targeting protein–protein interactions (PPIs) for therapeutic interventions has been an attractive strategy in drug discovery.[1,2] Because drug development for enzyme targets has been limited by the difficulties in achieving sufficient specificity, PPI inhibitors with extremely high specificity have recently attracted considerable attention. Despite advances in various techniques, such as nuclear magnetic resonance (NMR), surface plasma resonance (SPR), and fluorescence polarization (FP), the high-throughput screening (HTS) of small-molecule PPI inhibitors is highly challenging owing to several critical limitations: i) the large amount (mg quantities) of sample required for NMR;[3] ii) the low sensitivity of SPR for detection of small-molecule binding to proteins;[4,5] and iii) the requirement for fluorophore labeling in FP. Hence, there is a need to develop a robust HTS methodology to facilitate the discovery of small-molecule drugs against PPI targets.

Nanopore sensing is an emerging single-molecule technique for biomolecule analysis. When voltage is applied across a nanoscale pore, the translocation of a charged analyte through the nanopore transiently blocks the ionic current, which is characterized by dwell-time and current amplitude. Nanopore sensors have several unique advantages compared with more conventional techniques, including single-molecule resolution and ultrasensitivity, label-free and real-time measurements, and high-throughput detection.[6–12] Although nanopores have been used to characterize the biophysical properties of diverse biomolecules, including DNA, RNA, and proteins,[9–16] they have never been applied to the screening of small-molecule drugs such as PPI inhibitors.

Despite having much lower resolution and sensitivity, solid-state nanopores have advantages over biological protein nanopores, including high stability, a wide range of pore sizes, and controllable surface properties.[17,18] However, the problem of excess noise, which corresponds to a few tens of pA to 100 pA,[19,20] remains to be resolved. To improve the signal-to-noise ratio (SNR), we recently developed a solid-state nanopore platform with a sub-10 pA noise level by fabricating a SiN_x membrane directly on top of a highly insulating dielectric substrate, Pyrex.[20]

Blocking the interaction between mouse double minute 2 (MDM2) and p53 transactivation domain (p53TAD) has been an attractive strategy for cancer therapy because it can restore p53 function, resulting in cancer cell apoptosis. Using this therapeutic strategy, many p53TAD-mimetic lead compounds have been identified for cancer treatment. Among them, Nutlin-3 is one of the most potent MDM2 antagonists and acts as a competitive inhibitor of the MDM2/p53TAD interaction ($K_d = 0.1$ μM).[21,22] Nutlin-3 structurally mimics the 15-residue α-helical p53TAD peptide (residues Ser15–Asn29) that binds to MDM2.[23]

To probe the MDM2/p53TAD interaction and its small-molecule inhibition using solid-state nanopores, we fabricated ≈10–15 nm-sized nanopores in low-pressure chemical vapor deposition (LPCVD) SiN_x membranes transferred to the

[*] D.-K. Kwak,[+] Dr. M.-K. Lee,[+] Dr. J.-H. Ha, Dr. S.-W. Chi
Structural Biology & Nanopore Research Laboratory
Disease Target Structure Research Center, KRIBB
125 Gwahak-ro, Yuseong-gu, Daejeon 34141 (Republic of Korea)
E-mail: swchi@kribb.re.kr
D.-K. Kwak,[+] Dr. S.-W. Chi
Department of Bio-Analytical Sciences
Korea University of Science and Technology
217 Gajeong-ro, Yuseong-gu, Daejeon 34113 (Republic of Korea)
H. Chae,[+] Prof. K.-B. Kim
Department of Materials Science and Engineering
Seoul National University
599 Gwanak-ro, Gwanak-gu, Seoul 08826 (Republic of Korea)
E-mail: kibum@snu.ac.kr
Dr. G. Goyal, Prof. M. J. Kim
School of Biomedical Engineering
Science and Health Systems Drexel University
3701 Market Street, Philadelphia, PA 19104 (USA)
Prof. M. J. Kim
Department of Mechanical Engineering and Mechanics
Drexel University
3701 Market Street, Philadelphia, PA 19104 (USA)
[+] These authors contributed equally to this work.

Supporting information for this article can be found under: http://dx.doi.org/10.1002/anie.201511601.

Pyrex substrates.[20] The structure of the N-terminal p53TAD-binding domain of MDM2 (PDB code: 1YCR)[23] showed dimensions of 3.1 nm × 3.5 nm × 4.2 nm, (Figure 1a). At the applied voltage of −175 mV across the nanopore, the positively charged MDM2 domain (residues 3–109, net charge at pH 7.4 = + 2.9e, pI = 9.02) was electrophoretically driven from one chamber toward the negative electrode in the other chamber (Figure 1b). The passage of MDM2 through the nanopore gave rise to a temporary reduction in the ionic current, leading to the detection of MDM2 translocation events at the single-molecule level (Figure 1c). The ionic current was measured at a sampling rate of 250 kHz and filtered with a 10 kHz low-pass Bessel filter. Current traces were acquired with 100 nM MDM2 at an optimized electrolyte concentration of 1M KCl (Figure 1c). The translocation events were characterized by the dwell-time and the normalized blockade current ($\Delta I/I_0$; ΔI = magnitude of current drop, I_0 = open pore current). Figure 1e shows a scatter plot of the $\Delta I/I_0$ versus dwell-time of a total of 1372 MDM2 translocation events. Fitting the $\Delta I/I_0$ and dwell-time histograms to a lognormal function and a single exponential decay function (Figure 1f,g), respectively, yielded mean values of $\Delta I/I_0$ (0.016) and dwell-time (0.04 ms).

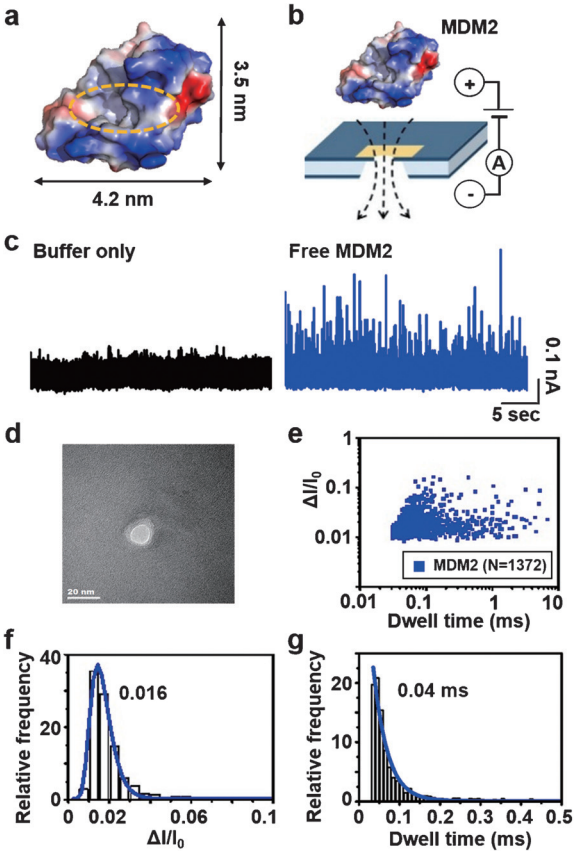

Figure 1. Nanopore-based analysis of MDM2 translocation events. a) Surface representation of the structure of free MDM2 (PDB code: 1YCR). Negatively and positively charged residues are indicated in red and blue, respectively. The p53TAD-binding pocket in MDM2 is indicated by the dotted yellow circle. b) Representation of MDM2 translocation. Positively charged MDM2 passes through a nanopore channel by negatively applied voltage. c) Current trace before and after addition of 100 nM MDM2 in 1M KCl and 1X PBS (pH 7.4) at an applied voltage of −175 mV. The ionic current root mean square (RMS) noise level (I_{RMS}) and SNR ($\Delta I/I_{RMS}$) were measured to be 17.5 pA and 13 at −175 mV, respectively. d) TEM image of a ≈10-nm diameter silicon nitride nanopore. e) Scatter plot of MDM2 translocation events at the −175 mV applied voltage. The translocation events are indicated by blue dots. Normalized current drop ($\Delta I/I_0$) (f) and dwell-time histograms (g) of MDM2 translocations were fitted using a lognormal function and a single exponential decay function, respectively. Mean values (≈0.016 and ≈0.04 ms) are indicated in histograms.

Of note, the SNR ($\Delta I/I_{RMS} \geq 13$) of our unique nanopore system was high enough to successfully detect the translocation of the small MDM2 domain (MW = 12.3 kDa) despite the very low magnitude current drops ($\Delta I/I_0 \cong 0.016$; Figure 1c). Because the high resistivity of Pyrex lowered the device capacitance and thus the high frequency noise, our application of the Pyrex substrate to the nanopore membrane considerably lowered the ionic current noise level (I_{RMS}) to sub-10 pA at 0 mV, which is nearly 10-times lower than that of the commonly used silicon-based nanopore device.[20]

Next, we detected the translocation of negatively charged 100 nM p53TAD (−14.2e at pH 7.4, pI = 3.6) at the applied voltage of + 100 mV (Figure 2a). To further improve the SNR of the current blockade caused by p53TAD (residues 1–73, MW = 8.2 kDa) translocation, we introduced a glutathione-S-transferase (GST) tag at the N-terminus of p53TAD. Increasing the molecular size of a protein without significantly changing its net charge can enhance the SNR of the current blockade signals caused by protein translocations. The GST tag is a relatively large protein (26.3 kDa) with a net charge of −2.9e at pH 7.4. As expected, the translocation of GST-p53TAD (−16.9e at pH 7.4) showed a dramatic increase in the magnitude of current blockade signals (Figure 2a,b). Thus, we used GST-p53TAD for our subsequent nanopore experiments.

Interestingly, the scatter plots displayed remarkably different distributions between p53TAD and GST-p53TAD (Figure 2c). Whereas GST-p53TAD translocation events are concentrated in the dwell-time of ≈0.1 ms, translocation events for intact p53TAD showed widely dispersed dwell-times ranging from 0.05 to 10 ms. In the histograms of dwell-time and $\Delta I/I_0$, p53TAD translocation events displayed a lower mean $\Delta I/I_0$ value (0.012) and increased mean dwell-time (0.13 ms) compared to those of GST-p53TAD, whose values were 0.037 ($\Delta I/I_0$) and 0.07 ms (dwell-time; Figure 2d–g). The p53TAD has been previously shown to be an intrinsically disordered protein (IDP) that is largely unfolded, but that can transiently form secondary structures in some regions.[24,25] On the other hand, GST-p53TAD is a mostly globular protein owing to the well-folded character of the large GST tag. The unfolded, linear conformation of p53TAD appears to substantially increase the dwell-time of translocation, and the uniquely wide distribution of the dwell-time reflects the conformational heterogeneity of the protein (Figure 2c). Taken together, nanopore analysis of p53TAD translocation suggests that structural differences between unfolded and folded proteins can be detected by a solid-state nanopore at the single-molecule level.

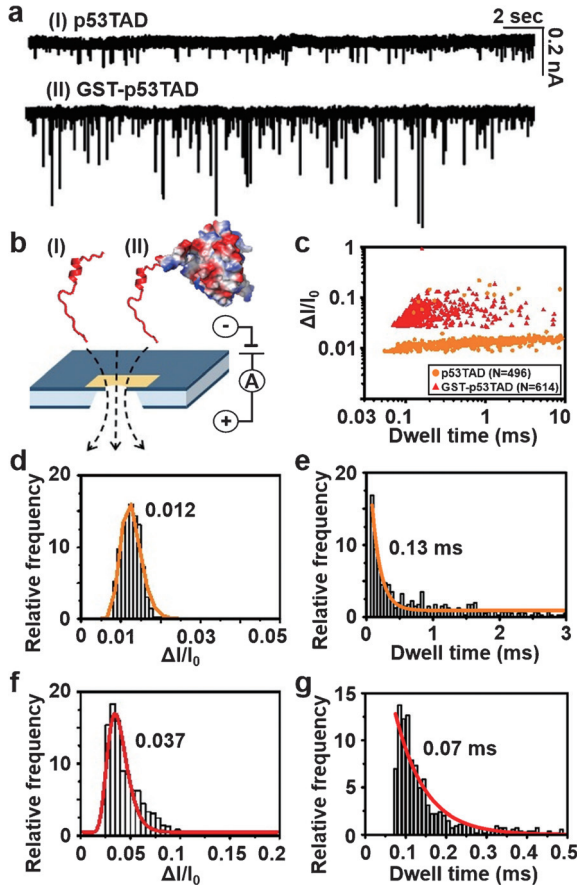

Figure 2. Nanopore-based analysis of p53TAD and GST-p53TAD translocation events. a) Current traces from p53TAD and GST-p53TAD translocations at the applied voltage of 100 mV. b) Representation of p53TAD (I) and GST-p53TAD (II) translocations through the nanopore. c) Scatter plots of p53TAD and GST-p53TAD translocation events. The p53TAD and GST-p53TAD translocation events are indicated as yellow circles and red triangles, respectively. Normalized current drop ($\Delta I/I_0$) (d) and dwell-time (e) histograms for p53TAD. Normalized current drop ($\Delta I/I_0$) (f) and dwell-time (g) histograms for GST-p53TAD. $\Delta I/I_0$ and dwell time data were fitted to a lognormal function and a single exponential decay function, respectively. Mean values are indicated in histograms. The concentration of each protein was 100 nM in 1 M KCl and 1X PBS (pH 7.4).

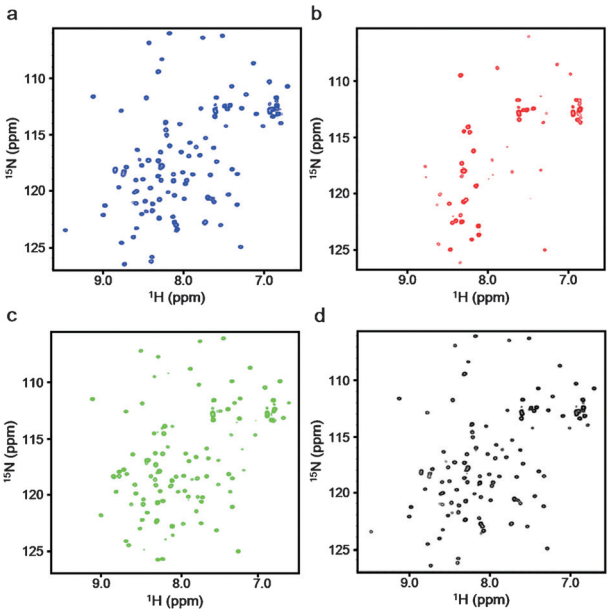

Figure 3. 2D ^{15}N-^{1}H HSQC spectra of free ^{15}N-labeled MDM2 protein (a), ^{15}N-labeled MDM2 complexed with unlabeled GST-p53TAD (molar ratio of 1:1) (b), ^{15}N-labeled MDM2 complexed with unlabeled GST-p53TAD and treated with Nutlin-3 (molar ratio of 1:1:1) (c), and ^{15}N-labeled MDM2 in the presence of unlabeled GST (molar ratio of 1:1) (d). The proteins and Nutlin-3 were mixed at a final concentration of 130 μM.

Prior to nanopore measurements, we examined the interaction between MDM2 and GST-p53TAD, as well as its small-molecule inhibition, using NMR spectroscopy. We recorded 2D ^{15}N-^{1}H heteronuclear single quantum correlation (HSQC) spectra of ^{15}N-labeled MDM2 in the absence or presence of GST-p53TAD (Figure 3a,b). When ^{15}N-labeled MDM2 was bound to GST-p53TAD, most of the ^{15}N-^{1}H crosspeaks in MDM2 disappeared owing to severe line broadening, indicating complex formation between MDM2 and GST-p53TAD. The binding of GST-p53TAD increased the tumbling time and decreased the T_2 relaxation time of the complex (Figure 3b). No such change was observed upon the addition of only GST (Figure 3d), indicating that GST alone did not bind to MDM2. Because a potent MDM2 antagonist, Nutlin-3, binds to the p53TAD-binding pocket of MDM2 with higher affinity than p53TAD does, it can disrupt the interaction between MDM2 and p53TAD ($K_d \cong 0.6$ μM). Expectedly, the addition of Nutlin-3 to the protein complex restored all of the missing crosspeaks of ^{15}N-labeled MDM2 (Figure 3c), suggesting that the binding of Nutlin-3 releases MDM2 from the complex. In addition, we performed the same experiments under 1M KCl (Supporting Information, Figure S1) and the results were essentially the same as that in Figure 3, confirming the binding between MDM2 and GST-p53TAD at the high salt concentration. Taken together, these results demonstrated the NMR-based detection of the PPI between MDM2 and GST-p53TAD and its competitive inhibition by Nutlin-3.

Following the same approach used for the NMR experiments, we monitored the interaction between MDM2 and GST-p53TAD and its inhibition by Nutlin-3 by using a Pyrex-based solid-state nanopore. Figure 4 shows the nanopore measurements of free MDM2 and the MDM2/GST-p53TAD complex in a system containing a ≈10 nm nanopore at the applied voltage of −175 mV. In contrast to the vigorous translocation of free MDM2, the number of translocation events for the MDM2/GST-p53TAD complex through the nanopore was dramatically reduced to a negligible level (Figure 4a). Upon complex formation, the net charge of the proteins at pH 7.4 changes from +2.9e (in free MDM2) to −13.7e (in the MDM2/GST-p53TAD complex) owing to charge masking of MDM2 by negatively charged GST-p53TAD. As a result, the overall negatively charged protein complex could not translocate through the nanopore at the applied negative voltage. This result prompted us to hypothesize that the association and dissociation of MDM2 and GST-

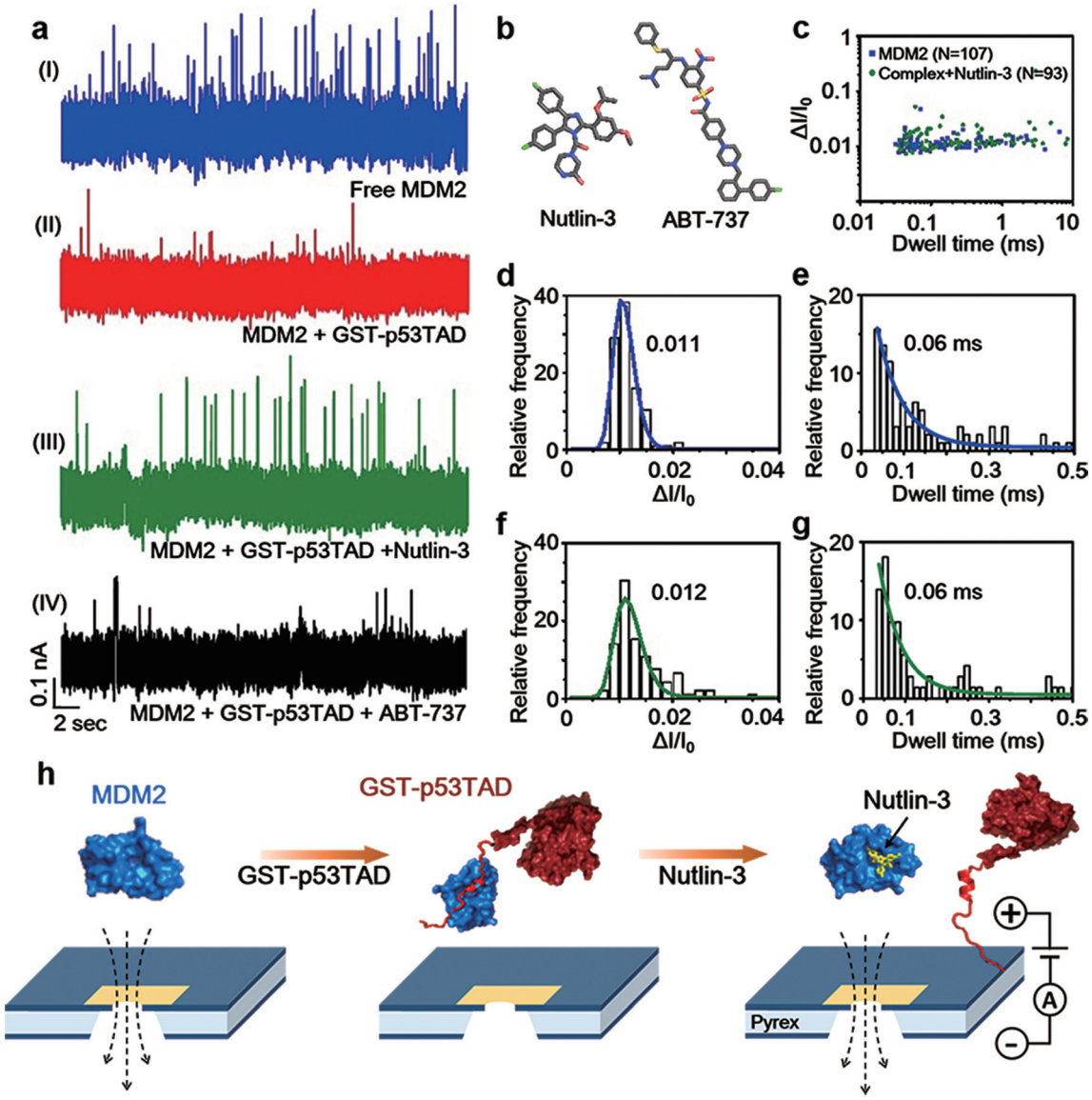

Figure 4. Nanopore-based detection of the MDM2-p53TAD interaction and its inhibition by Nutlin-3. a) Current traces from the translocations of free MDM2 (I), MDM2/GST-p53TAD complex (II; molar ratio of 1:1), and the complex with Nutlin-3 (III) or ABT-737 (IV; molar ratio of 1:1:1). b) Chemical structures of small molecules. c) Scatter plots of translocation events for free MDM2 and the complex treated with Nutlin-3. Translocation events for free MDM2 and recovered MDM2 are indicated as blue squares and green circles, respectively. d, e) $\Delta I/I_0$ and dwell-time histograms for free MDM2 translocation. f, g) $\Delta I/I_0$ and dwell-time histograms of the recovered MDM2 translocation by Nutlin-3. $\Delta I/I_0$ and dwell time data were fitted to a lognormal function and a single exponential decay function, respectively. Mean values are indicated in the histograms. h) Representation of the nanopore detection of MDM2/GST-p53TAD complex formation and PPI inhibition by Nutlin-3.

p53TAD could be monitored by using a solid-state nanopore at the picomole-scale.

To test this hypothesis, we measured the nanopore translocation of the MDM2/GST-p53TAD complex in the presence of Nutlin-3. After the addition of Nutlin-3 to the protein complex, the translocation of free MDM2 was almost recovered (Figure 4a), which indicated that the disruption of the MDM2/GST-p53TAD interaction by Nutlin-3 liberated MDM2 from the GST-p53TAD-bound complex (Figure 4h). The nanopore data statistics of free and Nutlin-3-recovered MDM2 translocations were analyzed and compared in Figure 4c–g. A scatter plot of current drop versus dwell-time for all translocation events revealed essentially the same distribution for the free and recovered MDM2 translocations. According to the histograms of current drop and dwell-time, both the free and recovered MDM2 translocation events have similar mean values of $\Delta I/I_0$ and dwell time; $\Delta I/I_0$ of 0.011 with a dwell-time of 0.06 ms and $\Delta I/I_0$ of 0.012 with a dwell-time of 0.06 ms for free and recovered MDM2, respectively (Figure 4d–g).

To test whether the MDM2/GST-p53TAD interaction is indeed specifically inhibited by Nutlin-3, we repeated the nanopore experiment with a negative control, ABT-737, which is an inhibitor of Bcl-2 family proteins and does not bind to MDM2. Unlike Nutlin-3, ABT-737 could not recover the translocation of MDM2 (Figure 4a,b), confirming that

Nutlin-3 specifically blocked the interaction between MDM2 and GST-p53TAD. In addition, no translocation event was observed for free Nutlin-3 and free ABT-737 at the same applied voltage (Figure S2).

To our knowledge, this result is the first demonstration of the application of solid-state nanopores to small-molecule drug screening. Compared with more conventional techniques that require labeling, immobilization, expensive instruments, and complicated procedures, the single-molecule-based nanopore system provides robust advantages for screening of small-molecule PPI inhibitors: i) ultrahigh sensitivity (10 picomole detection, ≈4500-fold higher sensitivity than NMR); ii) label-free and low-cost implementation; and iii) high-speed ($\leq$10 min) and small-volume ($\leq$100 μL) detection. These notable merits suggest that the nanopore-based drug screening platform is optimal for extension to HTS, which will be further accelerated by multi-array solid-state nanopores. Moreover, picomole-level detection by nanopores will enable screening with ultralow amounts of sample, which is extremely advantageous for insoluble small-molecule compounds and proteins.

In summary, we have probed the anticancer therapeutic MDM2/p53TAD interaction and its inhibition by the small molecule antagonist Nutlin-3 using solid-state nanopores. Our results provide a proof-of-concept for how solid-state nanopores can be a robust platform for the ultrasensitive, picomole-scale screening of small-molecule PPI inhibitors. This nanopore-based drug screening platform will provide a remarkable improvement over current technological limitations in drug discovery at protein–protein interfaces.

Acknowledgements

The authors thank Dr. Kyoung-Seok Ryu for helpful discussion on the manuscript. This work was supported by the National Research Foundation of Korea (NRF) grant funded by the Korean Government (MSIP) (NRF-2012M3C1A3671508) and by the Bio-Synergy Research Project of the Ministry of Science, ICT and Future Planning through the National Research Foundation (NRF-2015M3A9C4076320).

Keywords: drug screening · MDM2 · p53 · protein–protein interactions · solid-state nanopores

How to cite: *Angew. Chem. Int. Ed.* **2016**, *55*, 5713–5717
Angew. Chem. **2016**, *128*, 5807–5811

[1] J. A. Wells, C. L. McClendon, *Nature* **2007**, *450*, 1001–1009.
[2] M. R. Arkin, J. A. Wells, *Nat. Rev. Drug Discovery* **2004**, *3*, 301–317.
[3] H. Kovacs, D. Moskau, M. Spraul, *Prog. Nucl. Magn. Reson. Spectrosc.* **2005**, *46*, 131–155.
[4] P. Englebienne, A. V. Hoonacker, M. Verhas, *Spectroscopy* **2003**, *17*, 255–273.
[5] V. Perumal, U. Hashim, *J. Appl. Biomed.* **2014**, *12*, 1–15.
[6] A. J. Boersma, K. L. Brain, H. Bayley, *ACS Nano* **2012**, *6*, 5304–5308.
[7] L. Wang, Y. Han, S. Zhou, G. Wang, X. Guan, *ACS Appl. Mater. Interfaces* **2014**, *6*, 7334–7339.
[8] L. Wu, H. Liu, W. Zhao, L. Wang, C. Hou, Q. Liu, Z. Lu, *Nanoscale Res. Lett.* **2014**, *9*, 140.
[9] S. Carson, J. Wilson, A. Aksimentiev, M. Wanunu, *Biophys. J.* **2014**, *107*, 2381–2393.
[10] L. Q. Gu, M. Wanunu, M. X. Wang, L. McReynolds, Y. Wang, *Expert Rev. Mol. Diagn.* **2012**, *12*, 573–584.
[11] K. J. Freedman, S. R. Haq, M. R. Fletcher, J. P. Foley, P. Jemth, J. B. Edel, M. J. Kim, *ACS Nano* **2014**, *8*, 12238–12249.
[12] C. Plesa, S. W. Kowalczyk, R. Zinsmeester, A. Y. Grosberg, Y. Rabin, C. Dekker, *Nano Lett.* **2013**, *13*, 658–663.
[13] K. J. Freedman, S. R. Haq, J. B. Edel, P. Jemth, M. J. Kim, *Sci. Rep.* **2013**, *3*, 1638.
[14] K. J. Freedman, A. R. Bastian, I. Chaiken, M. J. Kim, *Small* **2013**, *9*, 750–759.
[15] M. Wanunu, T. Dadosh, V. Ray, J. Jin, L. McReynolds, M. Drndic, *Nat. Nanotechnol.* **2010**, *5*, 807–814.
[16] D. J. Niedzwiecki, C. J. Lanci, G. Shemer, P. S. Cheng, J. G. Saven, M. Drndic, *ACS Nano* **2015**, *9*, 8907–8915.
[17] A. J. Storm, J. H. Chen, X. S. Ling, H. W. Zandbergen, C. Dekker, *Nat. Mater.* **2003**, *2*, 537–540.
[18] M. J. Kim, M. Wanunu, D. C. Bell, A. Meller, *Nat. Nanotechnol.* **2006**, *18*, 3149–3153.
[19] S. Garaj, W. Hubbard, A. Reina, J. Kong, D. Branton, J. A. Golovchenko, *Nature* **2010**, *467*, 190–193.
[20] M. H. Lee, A. Kumar, K. B. Park, S. Y. Cho, H. M. Kim, M. C. Lim, Y. R. Kim, K. B. Kim, *Sci. Rep.* **2014**, *4*, 7448.
[21] S. W. Fesik, *Nat. Rev. Cancer* **2005**, *5*, 876–885.
[22] L. T. Vassilev, B. T. Vu, B. Graves, D. Carvajal, F. Podlaski, Z. Filipovic, N. Kong, U. Kammlott, C. Lukacs, C. Klein, N. Fotouhi, E. A. Liu, *Science* **2004**, *303*, 844–848.
[23] P. H. Kussie, S. Gorina, V. Marechal, B. Elenbaas, J. Moreau, A. J. Levine, N. P. Pavletich, *Science* **1996**, *274*, 948–953.
[24] S. Bell, C. Klein, L. Muller, S. Hansen, J. Buchner, *J. Mol. Biol.* **2002**, *322*, 917–927.
[25] M. Wells, H. Tidow, T. J. Rutherford, P. Markwick, M. R. Jensen, E. Mylonas, D. I. Svergun, M. Blackledge, A. R. Fersht, *Proc. Natl. Acad. Sci. USA* **2008**, *105*, 5762–5767.

Received: December 14, 2015
Revised: January 25, 2016
Published online: April 1, 2016

